Control of the Competition between a Magnetic Phase and a Superconducting Phase in Cobalt-Doped and Nickel-Doped NaFeAs Using Electron Count

Dinah R. Parker,[1] Matthew J. P. Smith,[1] Tom Lancaster,[2] Andrew J. Steele,[2] Isabel Franke,[2] Peter J. Baker,[3] Francis L. Pratt,[3] Michael J. Pitcher,[1] Stephen J. Blundell,[2,*] and Simon J. Clarke[1,†]

[1]*Department of Chemistry, University of Oxford, Inorganic Chemistry Laboratory, South Parks Road, Oxford, OX1 3QR, United Kingdom*

[2]*Clarendon Laboratory, Department of Physics, University of Oxford, Parks Road, Oxford OX1 3PU, United Kingdom*

[3]*ISIS Facility, STFC–Rutherford Appleton Laboratory, Harwell Science and Innovation Campus, Didcot, OX11 0QX, United Kingdom*

(Received 2 September 2009; published 5 February 2010)

Using a combination of neutron, muon, and synchrotron techniques we show how the magnetic state in NaFeAs can be tuned into superconductivity by replacing Fe by either Co or Ni. The electron count is the dominant factor, since Ni doping has double the effect of Co doping for the same doping level. We follow the structural, magnetic, and superconducting properties as a function of doping to show how the superconducting state evolves, concluding that the addition of 0.1 electrons per Fe atom is sufficient to traverse the superconducting domain, and that magnetic order coexists with superconductivity at doping levels less than 0.025 electrons per Fe atom.

DOI: 10.1103/PhysRevLett.104.057007 PACS numbers: 74.25.Ha, 74.62.−c, 74.90.+n, 76.75.+i

A primary challenge in understanding the high-temperature superconductivity exhibited by the newly discovered iron-arsenide compounds [1,2] is determining the hierarchy of effects that drive them from antiferromagnetic (AFM) order to superconductivity. This tuning can be achieved by changing the electron count [3], applying an external hydrostatic pressure [4], or making an isoelectronic chemical substitution which adjusts the structure (essentially applying a "chemical pressure" [5]). In order to constrain theoretical models of this phenomenon it is vital to assess the relative importance of electron count versus chemical pressure in model iron-arsenide systems. Phase diagrams have been extracted as a function of Co doping on the Fe site for the ternary "122" phases $Ba(Fe_{1-x}Co_x)_2As_2$ [3,6] and the quaternary "1111" phases $CaFe_{1-x}Co_xAsF$ [7], and as a function of F doping on the O site in $LnFeAsO_{1-x}F_x$ [8–10]. Although there are significant variations between different families, the magnetic and nonsuperconducting undoped parent material is always driven superconducting beyond a critical doping and exhibits a domelike superconducting region similar to that found in cuprates. The magnetic phase transition is normally preceded by a structural transition that does not occur in superconducting samples and coexistence between magnetic and superconducting phases is found in certain families [6,7,10].

The "111" compounds with formula AFeAs (A = Li, Na) and the anti-PbFCl structure type [see the inset of Fig. 1(b)] have emerged as a new series of ternary, chemically simple, iron arsenides. LiFeAs was shown to be a bulk superconductor in its undoped, stoichiometric form [11,12]. Stoichiometric NaFeAs [13] showed a 10% superconducting volume fraction and long-range AFM ordering in most of its volume [13]. These results imply that there might be some overlap between the AFM ordered and superconducting regions in the phase diagram in this material. In this Letter we map out this phase diagram for the chemically simpler compound NaFeAs upon substitution of Co and Ni for Fe. We follow the structural parameters in

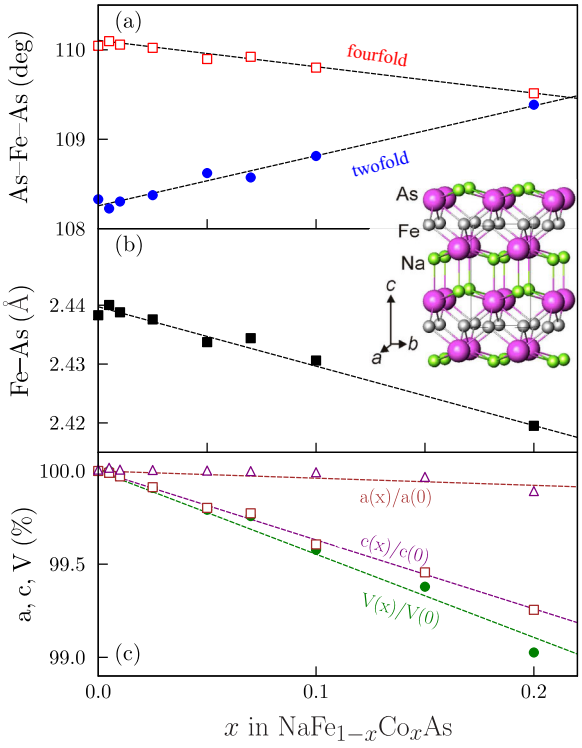

FIG. 1 (color online). The evolution at 298 K of (a) As–Fe–As bond angles, (b) Fe–As bond lengths, and (c) lattice parameters of $NaFe_{1-x}Co_xAs$ as a function of Co content. The lines are straight-line fits. Inset: Crystal structure of NaFeAs.

detail and demonstrate the exceptionally high sensitivity of the competition between magnetism and superconductivity to the electron count.

The compounds prepared were $NaFe_{1-x}Co_xAs$ ($x = 0, 0.005, 0.01, 0.025, 0.05, 0.07, 0.1, 0.15, 0.2$) and $NaFe_{1-x}Ni_xAs$ ($x = 0.025, 0.05, 0.1, 0.2$). All are extremely air sensitive and all manipulations of solids were performed in an argon-filled glovebox. The products were prepared from stoichiometric quantities of elemental reagents: freshly cut sodium pieces were placed in a 9 mm diameter Nb tube and a well-ground mixture of the transition metal and arsenic powders were placed on top. The tube was sealed under 1 atm of argon in an arc-welding furnace and heated at 200 °C in a resistance furnace for 48 h. The black initial product was extracted from the tube, homogenized in an agate mortar, and pressed into a pellet which was heated in a second sealed Nb tube at 750 °C for 48 h. The tube was cooled to room temperature in a few hours at the natural rate of the furnace. The final products were highly crystalline lustrous black powders and appeared phase pure according to the results of laboratory x-ray powder diffraction measurements.

Structural investigations were carried out using the high-resolution x-ray diffractometer ID31 at the ESRF, Grenoble, France, and the high-resolution neutron powder diffractometer HRPD at the ISIS facility, UK. On ID31 the samples were contained in 0.7 mm diameter glass capillary tubes sealed closed under helium exchange gas. Samples for neutron diffraction were contained in vanadium cylinders sealed with indium gaskets. Rietveld refinement was performed using the GSAS suite [14]. The diffraction data did not indicate more than 1%–2% Na deficiency, consistent with earlier reports [13,15]. The evolution of the lattice parameters and key structural parameters with composition at room temperature are summarized in Fig. 1. The $Fe(Co)As_4$ tetrahedra become more regular as Fe is substituted by Co [Fig. 1(a)] and the Fe(Co)–As bond distances decrease [Fig. 1(b)] as the smaller Co atom is substituted. The contraction in cell volume (by ≈1% between $x = 0$ and $x = 0.2$) is dominated by the contraction of the c lattice parameter [≈0.8% over this range of compositions, compared to ≈0.1% for the basal lattice parameter, a [Fig. 1(c)]]. A similar effect is found for Ni doping.

Magnetometry measurements were carried out using 30 mg samples on a Quantum Design MPMS-XL SQUID magnetometer under zero-field cooled and field cooled conditions in a measuring field of 5 mT. The evolution of the low temperature magnetic susceptibility with composition is shown in Fig. 2. The reported behavior of NaFeAs [13,16,17] is reproducible with several samples showing very small superconducting fractions (5%–10%) and broad superconducting transitions with T_c of around 10 K as judged from the onset of diamagnetism. Small levels of electron doping away from NaFeAs produce a rapidly

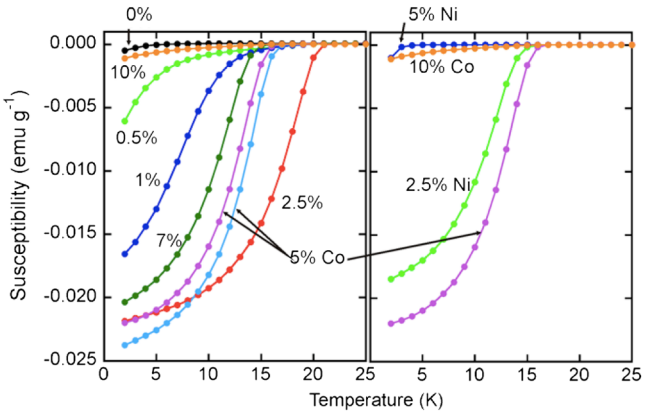

FIG. 2 (color online). The evolution of the zero-field magnetic susceptibility (measured in an applied magnetic field of 5 mT) of $Na_{1-x}Co_xAs$ samples (left) and the comparison of Ni- and Co-doped samples (right) showing that the susceptibilities are similar for isoelectronic compounds. Doping levels are expressed as percentages of Co unless specified.

increasing superconducting fraction. Co doping supplies one additional electron per Co atom and a fully superconducting state is attained between $NaFe_{0.975}Co_{0.025}As$ and $NaFe_{0.93}Co_{0.07}As$ with the maximum T_c of 21 K attained in $NaFe_{0.975}Co_{0.025}As$.

Substituting Ni for Co at an equivalent doping level doubles the amount of electron doping but produces a very similar doping dependence of lattice parameters. As shown in Fig. 2, the isoelectronic compounds $NaFe_{0.95}Co_{0.05}As$ and $NaFe_{0.975}Ni_{0.025}As$ exhibit extremely similar susceptibilities. Similarly, at the electron-rich boundary of the superconducting region, the isoelectronic $NaFe_{0.9}Co_{0.1}As$ and $NaFe_{0.95}Ni_{0.05}As$ both show very tiny superconducting fractions. These results strongly suggest that electron count, and hence band filling, is the key parameter which controls the superconductivity in this series of compounds. Samples with higher doping levels than 0.1 electrons per Fe did not exhibit superconductivity.

Zero-field muon-spin rotation (μSR) experiments were carried out on the GPS beam line at the Swiss Muon Source (SμS) in order to detect any magnetically ordered component or (see later) to probe the superfluid stiffness in any superconducting component. In NaFeAs, a clear oscillatory signal is observed [Fig. 3(a)] which can be fitted to an expression which is the sum of three components: $A(t) = \sum_{i=1}^{3} A_i \cos(2\pi\nu_i t)e^{-\lambda_i t}$. All three precession frequencies ν_i can be fitted and each follows a temperature dependence [Fig. 3(b)] consistent with a Néel temperature $T_N = 45.0(2)$ K and a critical exponent $\beta = 0.20(2)$. These results are consistent with AFM order with a primarily two-dimensional character. The relaxation rates λ_i stay roughly constant with temperature, but one of them (corresponding to the highest frequency component) diverges at T_N [Fig. 3(c)]. On substituting 1% of the Fe ions with Co to obtain a sample with a superconducting fraction of about

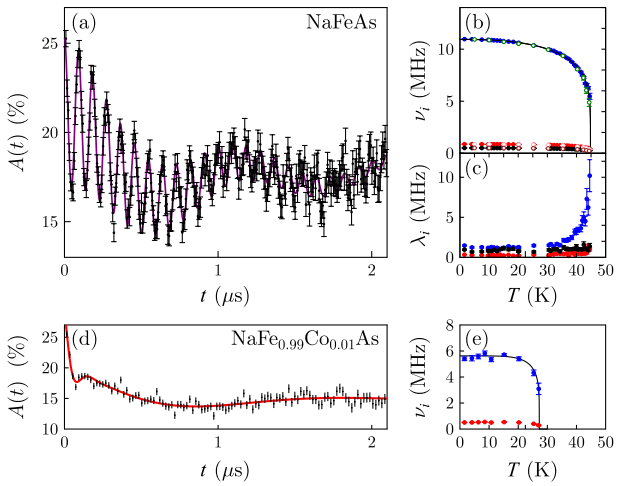

FIG. 3 (color online). (a) Zero-field μSR data in NaFeAs at 1.8 K. (b) Temperature dependence of the three precession frequencies (data for two different samples are shown in open symbols and closed symbols). (c) Relaxation rate for the three frequencies. (d) Zero-field μSR data in $NaFe_{0.99}Co_{0.01}As$ at 1.8 K and (e) temperature dependence of the precession frequencies (only two frequencies can be extracted in this case).

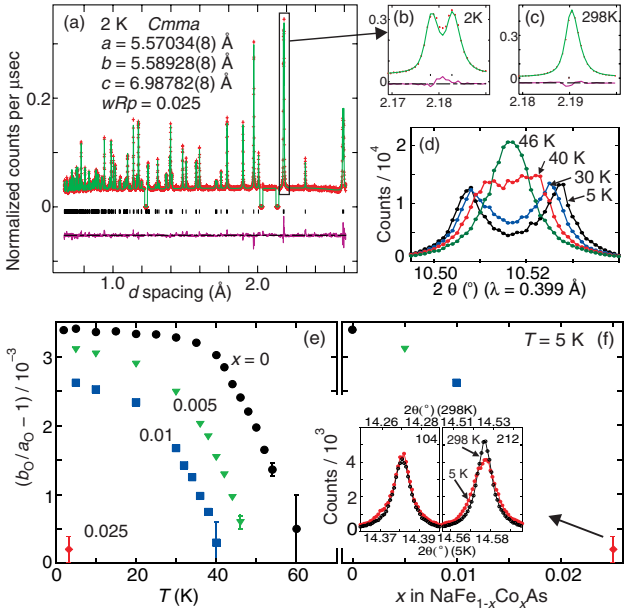

FIG. 4 (color online). (a) Rietveld refinements of NaFeAs against 2 K neutron data (HRPD). Data (red crosses), fit (green solid line), and difference plots are shown. Scattering from the sample environment has been excluded. (b),(c) Detail showing the splitting of the tetragonal 112 reflection into the orthorhombic 022 and 202 reflections. (d) Evolution of the orthorhombic 022/202 reflections in $NaFe_{0.995}Co_{0.005}As$ measured on ID31. At 46 K the orthorhombic and tetragonal models give fits of comparable quality. (e) Temperature dependence of the distortion for $NaFe_{1-x}Co_xAs$. The error bars lie within the points except when the presence of the distortion is marginal. (f) The size of the distortion at 5 K as a function of composition. Inset: For $NaFe_{0.975}Co_{0.025}As$ the tetragonal 212 reflection measured on ID31 at 5 K is broader than at room temperature while the tetragonal 104 reflection (orthorhombic 114) does not broaden.

60%, as judged by magnetometry, and a broad superconducting transition [Fig. 2], there is still evidence for long-range magnetic ordering in the sample, but the oscillations in the asymmetry are heavily damped [Fig. 3(d)] with lower frequency and T_N [Fig. 3(e)]. This implies a smaller internal field with a more inhomogeneous field distribution.

The undoped and lightly Co-doped samples were measured using high-resolution diffraction measurements at low temperatures. The nonsuperconducting "parent" phases of these arsenide superconductors commonly show a structural distortion driven by the long-range AFM ordering. Such a distortion was not evident in the original report on NaFeAs [13], but it was observed in a higher resolution study [15]. The distortion symmetry is similar to that in the "1111" and "122" parent phases with an orthorhombic $\sqrt{2}a_T \times \sqrt{2}a_T \times c_T$ cell of *Cmma* symmetry adopted at low temperatures (a_T and c_T are the tetragonal lattice parameters). The splitting of, for example, the 112 reflection in $P4/nmm$ into the 022 and 202 in *Cmma* is well resolved using HRPD [Figs. 4(a)–4(c)]. The high-resolution measurements show that in NaFeAs the distortion does not vanish until 55–60 K, well above T_N similar to the behavior observed for all classes of parent materials apart from the AFe_2As_2 (A = Ca, Sr, Ba) "122" series where the two transitions are coincident. Our measurements confirm that the two transitions identified by Chen *et al.* [16] at 41 and 52 K from heat capacity measurements correspond to the AFM-ordering transition at 45 K and the structural distortion at about 55 K.

In the lightly Co-doped regime $x \leq 0.01$ in which μSR shows that AFM ordering persists, diffraction measurements on the high-resolution powder diffractometer ID31 show that the distortion ($b_O/a_O - 1$, in terms of the basal plane orthorhombic lattice parameters) persists above T_N [Figs. 4(d) and 4(e)]. The size of the distortion at 5 K decreases smoothly with increasing Co content [Fig. 4(f)] showing a similar dependence on composition to T_N.

In iron-arsenide systems the structural distortion associated with AFM order is known to be quenched in the fully superconducting regime. Measurements at 5 K on ID31 of $NaFe_{0.975}Co_{0.025}As$, which lies in this regime, revealed broadening of the reflections which would split under an orthorhombic distortion, while reflections which would not split retained their ambient temperature widths [Fig. 4(f), inset]. At 5 K, the orthorhombic model refined stably but the goodness of fit was negligibly superior to that of the tetragonal model and the lattice parameters were clearly correlated with the peak profile parameters. An orthorhombic distortion may thus persist into the superconducting regime, although the upper bound on $b_O/a_O - 1$ is $3.0(1) \times 10^{-4}$ in $NaFe_{0.975}Co_{0.025}As$, an order of magni-

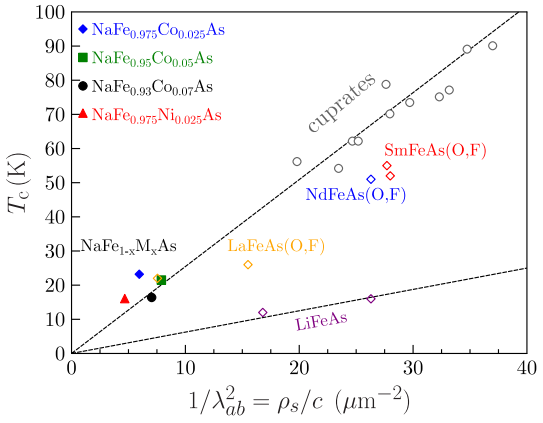

FIG. 5 (color online). Uemura plot of the superconducting transition temperature T_c versus the low temperature superfluid stiffness. Data obtained here for the doped NaFeAs samples are compared with previously reported data for other iron arsenides and cuprates [20–23]. The lower dashed line indicates the trend line for electron-doped cuprates, which closely corresponds to the behavior of the LiFeAs system [19], in contrast to the other iron-arsenide superconductors, which sit closer to the trend for hole-doped cuprates. The symbol size represents the typical estimated uncertainty of the data points.

tude smaller than in NaFeAs, and marginal even using an extremely high-resolution diffractometer.

Once a large superconducting fraction is established ($x \geq 0.025$) it is possible to use transverse-field μSR to study the superfluid stiffness by measuring the temperature and field dependence of the rms field broadening B_{rms} due to the vortex lattice [18]. Such experiments were performed using both SμS and the ISIS Pulsed Muon Facility and these data can be used to deduce the in-plane penetration depth λ_{ab} and superfluid stiffness ρ_s using $\rho_s/c = \lambda_{ab}^{-2} = (3/0.00371)^{1/2} B_{\mathrm{rms}}/\Phi_0$. Plotting our data on a Uemura plot (Fig. 5) demonstrates that the values of

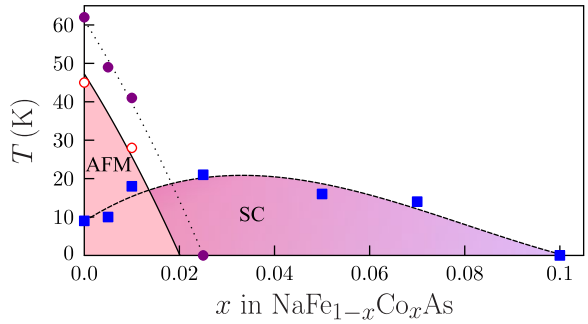

FIG. 6 (color online). Phase diagram for $NaFe_{1-x}Co_xAs$. The maximum temperature at which the distortion persists is shown by the filled circles and dotted line. The antiferromagnetic (AFM) phase is delineated by T_N (open circles) and superconducting (SC) phase by T_c (filled squares).

ρ_s correlate well with the trend observed in hole-doped cuprates and other iron arsenides, in contrast to the enhanced superfluid stiffness found for LiFeAs [19].

In conclusion, the parent compound NaFeAs lies just within a superconducting dome that can be traversed by the addition of 0.1 electrons per Fe atom and shows coexistence of antiferromagnetism and superconductivity over a region less than 0.025 electrons per Fe wide (see Fig. 6). While there are similarities with the phase diagrams of more complex iron-arsenide systems [3,6–10], the position of the parent compound is special in our case as coexistent superconductivity and magnetism is found without extrinsic doping. Since the structural effects of Co and Ni doping are very similar we are able to demonstrate the determinative role of electron count in controlling the physics of iron-arsenide layers.

We thank the EPSRC (U.K.) for financial support and STFC (U.K.) for access to ISIS and ESRF, K. S. Knight for assistance on HRPD, and A. N. Fitch and I. Margiolaki for assistance on ID31. Part of this work was performed at the Swiss Muon Source (SμS).

*s.blundell@physics.ox.ac.uk
†simon.clarke@chem.ox.ac.uk

[1] Y. Kamihara, T. Watanabe, M. Hirano, and H. Hosono, J. Am. Chem. Soc. **130**, 3296 (2008).
[2] K. Ishida, Y. Nakai, and H. Hosono, J. Phys. Soc. Jpn. **78**, 062001 (2009).
[3] P. C. Canfield *et al.*, Phys. Rev. B **80**, 060501(R) (2009).
[4] T. Park *et al.*, J. Phys. Condens. Matter **20**, 322204 (2008).
[5] C.-H. Lee *et al.*, J. Phys. Soc. Jpn. **77**, 083704 (2008).
[6] J.-H. Chu, J. G. Analytis, C. Kucharczyk, and I. R. Fisher, Phys. Rev. B **79**, 014506 (2009).
[7] S. Matsuishi *et al.*, J. Am. Chem. Soc. **130**, 14 428 (2008).
[8] J. Zhao *et al.*, Nature Mater. **7**, 953 (2008).
[9] H. Luetkens *et al.*, Nature Mater. **8**, 305 (2009).
[10] A. J. Drew *et al.*, Nature Mater. **8**, 310 (2009).
[11] M. J. Pitcher *et al.*, Chem. Commun. (Cambridge) 5918 (2008).
[12] J. H. Tapp *et al.*, Phys. Rev. B **78**, 060505(R) (2008).
[13] D. R. Parker *et al.*, Chem. Commun. (Cambridge) 2189 (2009).
[14] A. C. Larson and R. B. Von Dreele, Los Alamos National Laboratory Report No. LAUR 86-748, 2004.
[15] S. Li *et al.*, Phys. Rev. B **80**, 020504(R) (2009).
[16] G. F. Chen, W. Z. Hu, J. L. Luo, and N. L. Wang, Phys. Rev. Lett. **102**, 227004 (2009).
[17] C. W. Chu *et al.*, Physica (Amsterdam) **469C**, 326 (2009).
[18] J. E. Sonier, J. H. Brewer, and R. F. Kiefl, Rev. Mod. Phys. **72**, 769 (2000).
[19] F. L. Pratt *et al.*, Phys. Rev. B **79**, 052508 (2009).
[20] H. Luetkens *et al.*, Phys. Rev. Lett. **101**, 097009 (2008).
[21] A. J. Drew *et al.*, Phys. Rev. Lett. **101**, 097010 (2008); R. Khasanov *et al.*, Phys. Rev. B **78**, 092506 (2008).
[22] J. P. Carlo *et al.*, Phys. Rev. Lett. **102**, 087001 (2009).
[23] Y. J. Uemura, Physica (Amsterdam) **374B**, 1 (2006).